RSC Advances

PAPER

View Article Online
View Journal | View Issue

Cite this: *RSC Adv.*, 2016, **6**, 38499

Spin-dependent metallic properties of a functionalized MoS_2 monolayer†

Munish Sharma,*[ab] G. C. Loh,‡[b] Gaoxue Wang,[b] Ravindra Pandey,*[b] Shashi P. Karna[c] and P. K. Ahluwalia[a]

Received 7th March 2016
Accepted 11th April 2016

DOI: 10.1039/c6ra06083h

www.rsc.org/advances

Stability and electronic properties of a two-dimensional MoS_2 monolayer functionalized with atomic wires of Fe and Co are investigated using density functional theory. The binding energy of the atomic wires of Fe and Co on MoS_2 is noticeably higher relative to that calculated for the BN (0001) surface. The pristine monolayer is non-magnetic and semiconducting, and its functionalization makes the system magnetic and metallic. This is due to mainly the presence of a finite density of states associated with Fe or Co atoms in the vicinity of the Fermi level of the functionalized monolayer. Additionally, the spin-polarized character of the functionalized monolayer is clearly captured by the tunneling current calculated in the STM-like setup. We believe that the results form a basis for fabrication and characterization of such functionalized two-dimensional systems for applications at the nanoscale.

1. Introduction

The miniaturization of electronic devices with enhanced functionalities is the fundamental goal of current theoretical and experimental research in search of novel (two-dimensional) 2D materials.[1–3] The reason for the shift from bulk geometry towards low dimensional geometries is to enhance the carrier mobility in a single transistor and to have a large number of transistors on a single chip for faster switching operations and lower power consumption. Layered transition metal dichalcogenides (TMDs) with the chemical formula MX_2 (where, M is a metal atom and X is a chalcogen) have emerged as a new class of materials with interesting electronic properties.[4–7] They have a lamellar structure, similar to that of graphite, where individual layers are bonded *via* van der Waals interactions which are strong enough to hold them together but weak enough for them to be peeled off as quasi monolayers with three sub-layers. Furthermore, among the various TMDs, MoS_2 with an inherent band gap has been the prototype example showing a lot of promise for device applications.[8–11] For example, mobility of 200 $cm^2\ V^{-1}\ s^{-1}$ at room temperature can be achieved in MoS_2 monolayer using hafnium oxide (HfO_2) as the gate dielectric, thereby making it to be competitor of graphene nano-ribbons.[12]

In order to induce magnetism in non-magnetic materials, adsorption and doping of transition metal atoms appear to be effective ways.[10,13–18] For example, ferromagnetism on Pt surface was induced by deposition of atomic chains of Co.[19] Similarly, half-metallic character of the wurtzite BN (0001) surface functionalized with the atomic chains of transition metals (*e.g.* Fe, Co and Ni) was predicted.[20] Another theoretical study explored the effect of substrate including (110) surfaces of Cu, Pd, Ag, and NiAl on the magnetic coupling in transition metal atomic chains.[21] The functionalization of MoS_2 monolayer by adatoms and vacancies have been previously investigated,[22] and our group has studied the effect of nonmagnetic atomic nanowires on the electronic properties of MoS_2.[23]

Inspired by these results, we now look into inducing spin-dependent metallic properties in the semiconducting MoS_2 monolayer *via* its functionalization by monoatomic wires of Fe and Co which has not been explored so far. The electronic configurations of Fe and Co are [Ar] 3 d^6 4 s^2 and [Ar] 3 d^7 4 s^2, respectively. The objectives of the present investigation is to study: (i) stability of ferromagnetic and anti-ferromagnetic Fe and Co atomic wires on pristine MoS_2, (ii) modification in the electronic band structures upon functionalization, (iii) induced magnetization in MoS_2 upon functionalization, (iv) spin dependent tunneling current characteristics of Fe (Co) functionalized MoS_2.

2. Computational method

Spin polarized electronic structure calculations were performed within the framework of density functional theory (DFT) using

[a]*Department of Physics, Himachal Pradesh University, Shimla 171005, India. E-mail: munishsharmahpu@live.com*

[b]*Department of Physics, Michigan Technological University, Houghton, Michigan 49931, USA. E-mail: pandey@mtu.edu*

[c]*US Army Research Laboratory, Weapons and Materials Research Directorate, ATTN: RDRL-WM, Aberdeen Proving Ground, MD 21005-5069, USA*

† Electronic supplementary information (ESI) available. See DOI: 10.1039/c6ra06083h

‡ Permanent address: Institute of High Performance Computing, 1 Fusionopolis Way, #16-16 Connexis, Singapore 138632.

the projector augmented-wave (PAW) method,[24] as implemented in the Vienna *ab initio* simulation package (VASP).[25,26] The exchange and correlation effects were treated within the generalized gradient approximation (GGA) using Perdew and Wang (PW91) functional.[27] The van der Waals interactions resulting from dynamical correlations between fluctuating charge distribution was described within the Tkatchenko–Scheffler method.[28] Due to the relatively small spin–orbit coupling (SOC) in MoS_2 compared to other transition metal dichalcogenides,[29] the SOC is not included in the calculation and it is expected to have very limited effect on the adsorption of atomic wires on MoS_2.

The pristine MoS_2 monolayer was simulated by a periodic supercell. For the functionalized monolayer, the lattice mismatch between atomic wire and MoS_2 and the wire–wire interaction in the periodic system were minimized. For example, the calculated lattice mismatch is +3% and −1.3% for Fe/MoS_2 and Co/MoS_2 by taking a supercell of $(5 \times 5 \times 1)$ for MoS_2 and $(1 \times 4 \times 1)$ for the 1-dimensional linear atomic wire. This choice also led to the negligible wire–wire interaction in periodic images with distance larger than 16 Å. Also, a vacuum distance of 25 Å along the *z*-direction was used to ensure negligible interactions between 2D system images. The Monkhorst–Pack scheme with a *k* mesh of $(15 \times 15 \times 1)$ was used for the functionalized monolayer. The electronic density of states (DOS) was calculated with Gaussian broadening parameter of 0.1 eV. The energy convergence criterion of 10^{-6} eV was used for self-consistency for electronic steps. The structure was relaxed using the conjugate gradient method with force on each atom less than 0.01 eV $Å^{-1}$.

3. Results and discussion

In order to benchmark the modeling elements, we have calculated the structural and electronic properties of the freestanding atomic wires and the pristine MoS_2 monolayer which show an excellent agreement with previously reported theoretical and experimental values. For example, the calculated lattice parameters of the pristine monolayer are in close agreement with the values obtained using density functional theory[15,22,30,31] and experimentally measured values.[4,32–34] For the monolayer, $R_{(Mo–S)}$ is 2.42 Å, $R_{(S–S)}$ is 3.12 Å, $A_{(S–Mo–S)}$ is 80.51°, and the lattice constant is 3.18 Å. The spin-polarized electronic band structure shows MoS_2 to be semiconductor with a direct band gap of 1.59 eV at K point. The calculated band gap is underestimated as compared to experimentally measured values[4,33] following the well-known deficiency of DFT level of theory. Most of the contributions to the valance band maximum (VBM) and conduction band minimum (CBM) originates from Mo atoms including Mo-d_{z^2} and Mo-$d_{x^2-y^2}$ orbitals. A symmetric density of states for spin-up and spin-down states confirms MoS_2 to be nonmagnetic in its pristine form (see ESI, Fig. S1†).

In the freestanding atomic wires, the asymmetric spin-up and spin-down total density of states suggests the presence of magnetic order in the monatomic Fe and Co wires. The ground state of the Fe (Co) atomic wire is ferromagnetic (FM) with energy 10 (590) meV lower than that of anti-ferromagnetic state (AFM) (see ESI, Fig. S2 and S3†). The magnetic moment per atom in linear wires is found to be 2.92 μ_B/Fe and 2.03 μ_B/Co. The calculated near-neighbor distance is 1.94 and 2.02 Å for Fe and Co linear wires, respectively. In the functionalized monolayer, there exists a strain of +3% and −1.3% in Fe and Co wires, respectively due to lattice mismatch. The calculated magnetic moments and the spin resolved total density of states nearly remain the same for the strained Fe and Co atomic wires (Fig. S3†).

There exist several binding sites on the monolayer for the linear wire which are shown in Fig. 1.

To ascertain the preferred configuration of the functionalized monolayer, the binding energy (E_b) is calculated as follows:

$$E_b = [E_{wire@MoS_2} - (E_{wire} + E_{MoS_2})]/n, \quad (1)$$

where *n* is the number of atoms in the atomic wire, $E_{wire@MoS_2}$ is the total energy of the functionalized system, E_{wire} and E_{MoS_2} are the total energy of the strained wire and MoS_2 monolayer, respectively.

Fig. 2 displays the E_b as a function of separation between atomic wire and the monolayer (*i.e.* ($d_{wire@MoS_2}$)) for the binding configurations, namely (i) top of the Mo atom (*i.e.* top (Mo)), top of the S atom (*i.e.* top (S)), (iii) top of the Mo–S bond (*i.e.* bridge (Mo–S)), (iv) top of the S–S bond (*i.e.* bridge (S–S)), and (v) top of the hexagonal ring (*i.e.* hollow (HR)) sites (see ESI, Fig. S4 and Table S1†).

The calculated results find the bridge (S–S) configuration to be the preferred site with E_b of ∼0.5 eV for both Fe/MoS_2 and Co/MoS_2 functionalized monolayers. The separation between atoms of the wire and S atoms of the monolayer ($d_{wire@MoS_2}$) is calculated to be 1.50 Å. Here, Fe (Co) atoms of the linear wires transfer a fraction of Bader's charge ∼0.24 e per atom to S atoms of the monolayer[35] (see ESI, Table S2†). Additionally, the charge density difference profiles (defined by $\Delta\rho_{wire@MoS_2} = \rho_{wire@MoS_2} - \rho_{MoS_2} - \rho_{wire}$) show that charge redistribution is more pronounced in the region between atomic wire and upper layer

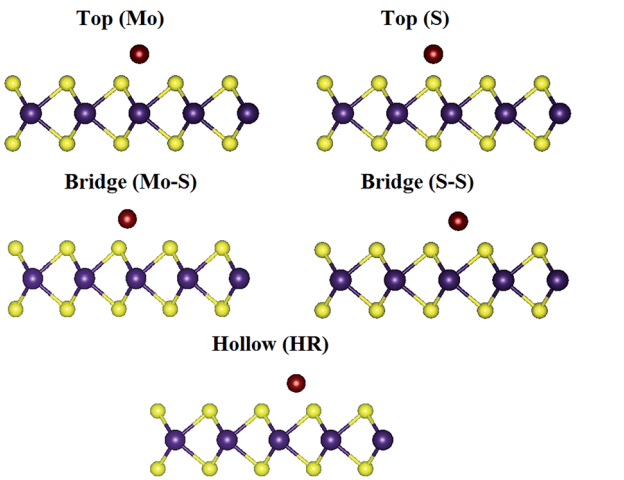

Fig. 1 A ball and stick model of the functionalized monolayer showing side views of binding sites. The violet, yellow and brown balls represent Mo, S and Fe/Co atoms, respectively.

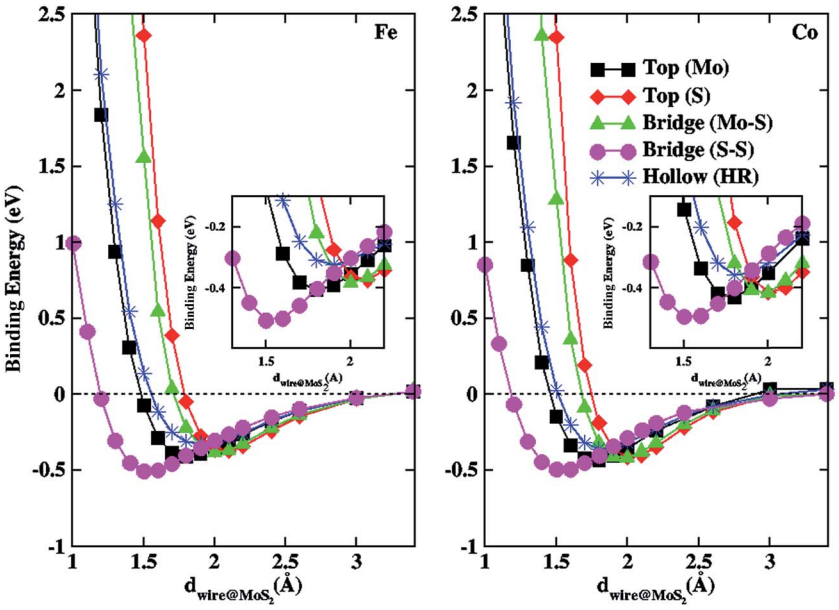

Fig. 2 Binding energy as a function of separation ($d_{wire@MoS_2}$) between wire and MoS_2.

of MoS_2 (Fig. 3). Both Fe/MoS_2 and Co/MoS_2 have similar charge redistribution which supports the inference drawn for the similar binding energy values for the functionalized monolayers (see ESI, Table S1†).

In order to confirm the predicted stability of the functionalized MoS_2 in the ferromagnetic (FM) configuration, the spin-polarized electronic structure calculations were performed on the anti-ferromagnetic (AFM) configurations of both Fe and Co functionalized MoS_2 monolayers. The difference in energy of the FM and AFM configurations is calculated to be 15 and 313 meV for Fe and Co functionalized monolayers, respectively. In the AFM configuration, the calculated binding energy is +1.58 eV and −0.47 eV for Fe and Co functionalized monolayers, respectively. Note that a positive value of the binding energy indicates instability of the AFM configuration of the Fe functionalized MoS_2.

In the functionalized monolayers, modifications in the electronic density lead to introduction of new states near the Fermi energy in the band structure making them to be metallic (Fig. 4 and S5†). These additional bands appear to be associated with atomic wires and are dominated by the spin-down states.

The metallicity of the functionalized monolayer is further confirmed by the total and projected density of states as shown in Fig. 5 and 6, respectively. The presence of finite spin up and spin down density of states in the vicinity of Fermi energy confirms the metallic nature of functionalized monolayer. The difference in spin up and spin down total density of states gives clear signature of presence of magnetic order. In the pristine monolayer, both spin up and spin down states near Fermi energy are dominated by Mo-d states. On the other hand, Co-d states contribute to both spin up and spin down states near Fermi energy for Co/MoS_2. This is not the case with Fe/MoS_2 where spin-up states projected on Fe-d orbitals appear to vanish near Fermi energy. This difference can be attributed to availability of additional d-electron for Co as compared to Fe in the functionalized monolayer.

Next, we turn to determine the magnetic properties of the functionalized monolayers. The calculated values of the magnetic moment per atom are 2.75 and 1.55 μ_B for Fe/MoS_2 and Co/MoS_2, respectively. Note that the monolayer remains non-magnetic as revealed by the spin density plots (see ESI, Fig. S6†). Considering that the calculated magnetic moment per atom is 2.99 μ_B and 2.03 μ_B for the strained freestanding Fe and Co atomic wires, overlap of Fe-d and Co-d with S-p orbitals appears to decrease the magnetic moment of Fe and Co atomic wire. We notice that the magnitude of quenching in Co is higher than that in Fe due to availability of an additional d-electron in Co which facilitates significant hybridization with S-p electrons

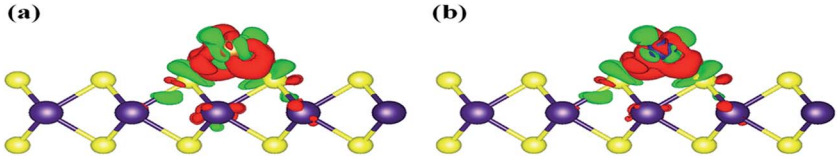

Fig. 3 Charge density difference plots for (a) Fe-functionalized MoS_2 (b) Co-functionalized MoS_2. Green and red color represents charge accumulation and depletion respectively. The isosurface values are set at 0.004 e $Å^{-3}$.

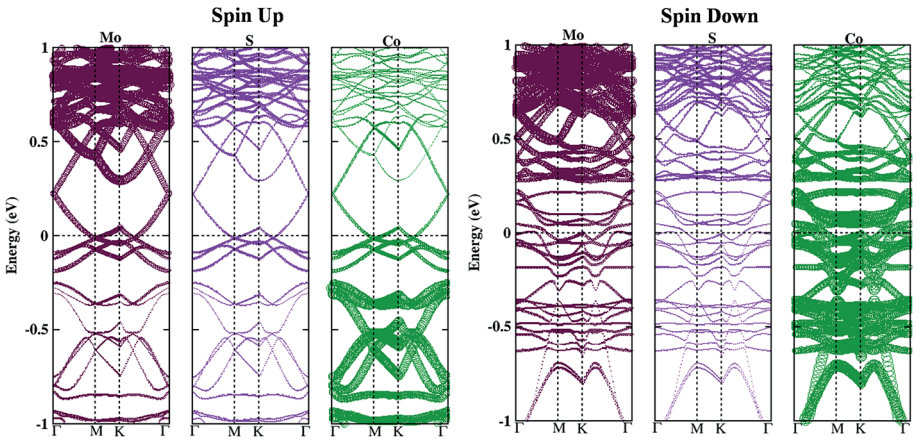

Fig. 4 Projected spin-polarized band structures of the Co functionalized monolayer. The width of the bands depicts spectral weight of the points. Fermi energy is set at 0 eV.

of the monolayer. Our results follow the trend exhibited by adsorption of a single Fe (Co) atom on the MoS_2 monolayer[15] for which the respective values are 2.44 and 0.77 μ_B (see ESI, Table S3†).

In the functionalized monolayers, the presence of finite density of states near the Fermi level is expected to modify electron transport properties relative to the pristine semiconducting monolayer. This expected increase in conductance can be quantified by calculating the current–voltage characteristics within the scanning tunneling microscope (STM) measurements.[35] In the STM-like setup, a spin-polarized tip is modeled by a ferromagnetic cage-like Fe_{13} cluster. Since the ferromagnetic and anti-ferromagnetic nature of Fe tip is still not established, it was assumed that an excess of Fe at the apex of the tip results in the induced ferromagnetism in STM experiments.[36] The Bardeen, Tersoff and Hamann (BTH) formalism[37,38] has been successfully used to simulate tunneling characteristics of nanostructures including BN monolayer phosphorene and molybdenum disulphide.[23,39–43]

We define the biasing to be forward bias (or positive bias) when the sample is connected to the positive potential with electrons flowing from tip to sample. The separation between the tip and the monolayer is taken to be 3 Å. It is worth mentioning here that the choice of the tip and sample separation defines the magnitude of current, although the tunneling characteristics remain the same.

The spin-polarized tunneling current characteristics for the pristine and functionalized MoS_2 are given in Fig. 7. The functionalized monolayers show ohmic-like characteristics up to a small positive bias of ~0.1 V. In the reverse bias, an asymmetric variation in current is predicted. Also, a relatively large magnitude of tunneling current is predicted for Co/MoS_2 as compared to Fe/MoS_2. The nearly zero current in the bias range of −0.5 V to +0.5 V is calculated for the pristine semiconducting monolayer.

As the tunneling current is directly proportional to the convolution of DOS between the tip and sample, the finite spin-

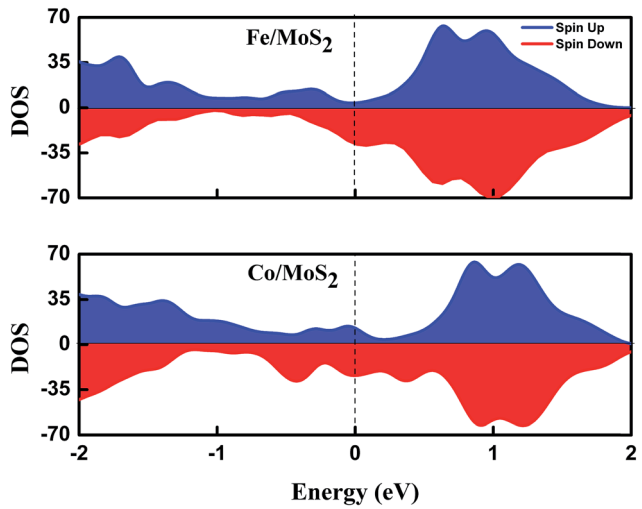

Fig. 5 Spin-polarized total density of states of the functionalized monolayers. Fermi energy is set at 0 eV.

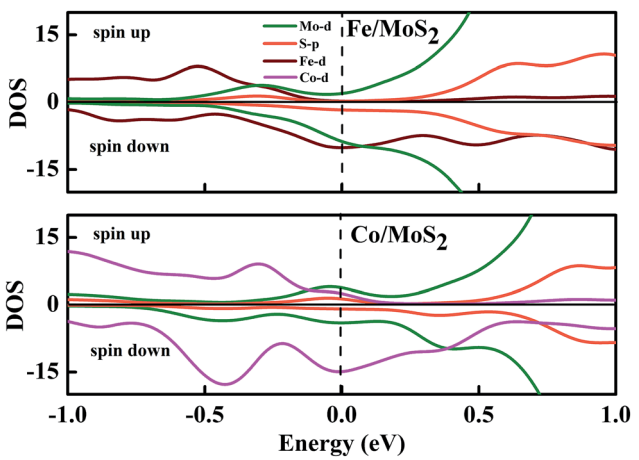

Fig. 6 Spin-polarized projected density of states for the functionalized monolayers. Fermi energy is set at 0 eV.

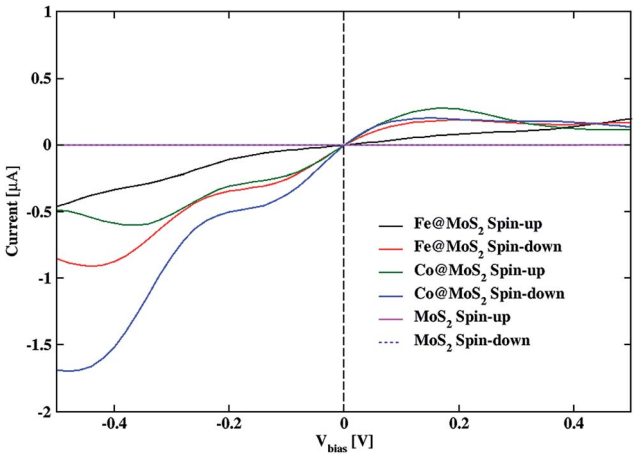

Fig. 7 Spin-polarized *I*–*V* characteristics of the functionalized monolayers.

up and spin-down DOS in the vicinity of the Fermi level of the functionalized monolayer is likely the reason of increase in tunneling of both spin carriers (spin-up and spin-down) with the bias voltage. An additional d-electron in Co atom as compared to Fe atom leads to increase in density of states which results in an increase in the tunneling current. It is interesting to note that the magnitude of tunneling current increases in negative bias as compared to positive bias which can be attributed to the larger number of unoccupied states in the functionalized monolayers (Fig. 4 and S5†).

It is worth mentioning here that stability of clusters and atomic wires of Fe and Co on graphene[44] and BN (0001) surface,[20] respectively have previously been investigated. For example, stability of atomic wires of Fe and Co on BN (0001) surface have been predicted with a binding energy of about 1 eV.[20] On the other hand, clusters of Fe and Co are reported to have binding energies of 0.88 and 2.14 eV, respectively. Our results therefore, find a noticeable higher binding energy for atomic wires of Fe and Co on a MoS_2 monolayer. This is also the case with our previous studies of stability of atomic wires of noble metals interacting with MoS_2.[23] Fe or Co atomic wire induced metallicity in MoS_2 is in line with previous reports on the functionalization of MoS_2 or BN surface by metallic nanowires.[20,23]

4. Summary

Stability and electronic properties of the functionalized MoS_2 monolayers are investigated using density functional theory. The binding energy of atomic wires of Fe and Co on MoS_2 as compared to previously investigated BN (0001) surface.[20] The pristine monolayer is non-magnetic and semiconducting, and its functionalization with ferromagnetic Fe and Co linear atomic wires makes composite system to be magnetic and metallic. This is further confirmed by the calculated tunneling currents showing ohmic-like characteristics for the low bias in the functionalized MoS_2 monolayers. Additionally, appearance of unoccupied spin-down states in the vicinity of Fermi level leads to enhanced conductance in the reverse bias as compared to the forward bias in the functionalized MoS_2 monolayers. We believe that the results provide a significant addition to the existing knowledge of the functionalized MoS_2 monolayers and form a basis for further investigations of such assembled systems for applications in electronic devices at nanoscale.

Acknowledgements

Helpful discussions with Dr Ashok Kumar, William Slough, Kevin Waters and Kriti Tyagi are acknowledged. The authors thank Dr Douglas Banyai for providing his STM simulation code. Financial support from ARL W911NF-14-2-0088 is acknowledged. MS wishes to acknowledge the DST, govt. of India, New Delhi for providing the financial support in the form of INSPIRE Fellowship. RAMA and SUPERIOR, high performance computing clusters at Michigan Technological University were used in obtaining the results presented in this paper. CVRAMAN, high performance computing cluster at Himachal Pradesh University has been used to obtain part of results presented in this paper.

References

1 X. Tong, E. Ashalley, F. Lin, H. Li and Z. M. Wang, *Nano-Micro Lett.*, 2015, 1–16.
2 R. Ganatra and Q. Zhang, *ACS Nano*, 2014, **8**, 4074–4099.
3 G. Han and Y. Yoon, *Appl. Phys. Lett.*, 2014, **105**, 213508.
4 K. F. Mak, C. Lee, J. Hone, J. Shan and T. F. Heinz, *Phys. Rev. Lett.*, 2010, **105**, 136805.
5 A. Yoffe, *Annu. Rev. Mater. Sci.*, 1973, **3**, 147–170.
6 A. Kumar and P. K. Ahluwalia, *Eur. Phys. J. B*, 2012, **85**, 1–7.
7 M. Sharma, A. Kumar, P. K. Ahluwalia and R. Pandey, *J. Appl. Phys.*, 2014, **116**, 063711.
8 Z. M. Wang, *MoS2: Materials, Physics, and Devices*, Springer Science & Business Media, 2013.
9 Q. H. Wang, K. Kalantar-Zadeh, A. Kis, J. N. Coleman and M. S. Strano, *Nat. Nanotechnol.*, 2012, **7**, 699–712.
10 A. Ramasubramaniam and D. Naveh, *Phys. Rev. B: Condens. Matter Mater. Phys.*, 2013, **87**, 195201.
11 Y. Morita, T. Onodera, A. Suzuki, R. Sahnoun, M. Koyama, H. Tsuboi, N. Hatakeyama, A. Endou, H. Takaba and M. Kubo, *Appl. Surf. Sci.*, 2008, **254**, 7618–7621.
12 B. Radisavljevic, A. Radenovic, J. Brivio, V. Giacometti and A. Kis, *Nat. Nanotechnol.*, 2011, **6**, 147–150.
13 K. T. Chan, J. Neaton and M. L. Cohen, *Phys. Rev. B: Condens. Matter Mater. Phys.*, 2008, **77**, 235430.
14 W. Cong, Z. Tang, X. Zhao and J. Chu, *Sci. Rep.*, 2015, **5**, 9361.
15 Y. Wang, B. Wang, R. Huang, B. Gao, F. Kong and Q. Zhang, *Phys. E*, 2014, **63**, 276–282.
16 M. Yin, X. Wang, W. Mi and B. Yang, *Comput. Mater. Sci.*, 2015, **99**, 326–335.
17 X. Zhang, W. Mi, X. Wang, Y. Cheng and U. Schwingenschlögl, *Sci. Rep.*, 2014, **4**, 7368.
18 N. Feng, W. Mi, Y. Cheng, Z. Guo, U. Schwingenschlögl and H. Bai, *ACS Appl. Mater. Interfaces*, 2014, **6**, 4587–4594.

19 P. Gambardella, A. Dallmeyer, K. Maiti, M. Malagoli, W. Eberhardt, K. Kern and C. Carbone, *Nature*, 2002, **416**, 301–304.
20 S. Luo, G. Guo and A. Laref, *J. Phys. Chem. C*, 2009, **113**, 14615–14622.
21 Y. Mokrousov, G. Bihlmayer, S. Blügel and S. Heinze, *Phys. Rev. B: Condens. Matter Mater. Phys.*, 2007, **75**, 104413.
22 C. Ataca and S. Ciraci, *J. Phys. Chem. C*, 2011, **115**, 13303–13311.
23 A. Kumar, D. Banyai, P. Ahluwalia, R. Pandey and S. P. Karna, *Phys. Chem. Chem. Phys.*, 2014, **16**, 20157–20163.
24 P. E. Blöchl, *Phys. Rev. B: Condens. Matter Mater. Phys.*, 1994, **50**, 17953.
25 G. Kresse and J. Furthmüller, *Comput. Mater. Sci.*, 1996, **6**, 15–50.
26 G. Kresse and D. Joubert, *Phys. Rev. B: Condens. Matter Mater. Phys.*, 1999, **59**, 1758–1775.
27 J. P. Perdew, P. Ziesche and H. Eschrig, *Electronic structure of solids' 91*, Akademie Verlag, Berlin, 1991.
28 A. M. V. D. W. Interactions, *Phys. Rev. Lett.*, 2009, **102**, 073005.
29 Z. Y. Zhu, Y. C. Cheng and U. Schwingenschlögl, *Phys. Rev. B: Condens. Matter Mater. Phys.*, 2011, **84**, 153402.
30 T. Li, *Phys. Rev. B: Condens. Matter Mater. Phys.*, 2012, **85**, 235407.
31 X. Zhang, X. Wang and W. Mi, *Solid State Commun.*, 2015, **212**, 35–40.
32 P. Joensen, E. Crozier, N. Alberding and R. Frindt, *J. Phys. C: Solid State Phys.*, 1987, **20**, 4043.
33 A. Splendiani, L. Sun, Y. Zhang, T. Li, J. Kim, C.-Y. Chim, G. Galli and F. Wang, *Nano Lett.*, 2010, **10**, 1271–1275.
34 D. Yang, S. J. Sandoval, W. Divigalpitiya, J. Irwin and R. Frindt, *Phys. Rev. B: Condens. Matter Mater. Phys.*, 1991, **43**, 12053.
35 D. Tománek and S. G. Louie, *Phys. Rev. B: Condens. Matter Mater. Phys.*, 1988, **37**, 8327.
36 U. R. Singh, R. Aluru, Y. Liu, C. Lin and P. Wahl, *Phys. Rev. B: Condens. Matter Mater. Phys.*, 2015, **91**, 161111.
37 J. Tersoff and D. Hamann, *Phys. Rev. Lett.*, 1983, **50**, 1998.
38 R. M. Feenstra, J. A. Stroscio and A. Fein, *Surf. Sci.*, 1987, **181**, 295–306.
39 H. He, R. Pandey, R. Pati and S. P. Karna, *Phys. Rev. B: Condens. Matter Mater. Phys.*, 2006, **73**, 195311.
40 S. K. Gupta, H. He, D. Banyai, M. Si, R. Pandey and S. P. Karna, *Nanoscale*, 2014, **6**, 5526–5531.
41 G. Wang, R. Pandey and S. P. Karna, *Nanoscale*, 2015, **7**, 524–531.
42 G. Wang, R. Pandey and S. P. Karna, *ACS Appl. Mater. Interfaces*, 2015, **7**, 11490–11496.
43 G. Wang, R. Pandey and S. P. Karna, *Appl. Phys. Lett.*, 2015, **106**, 173104.
44 S. Sahoo, M. E. Gruner, S. N. Khanna and P. Entel, *J. Chem. Phys.*, 2014, **141**, 074707.